Electrical and optical properties of materials
John JL Morton

Part 1. Conductivity: from insulators to superconductors

We will begin this lecture course with an overview of the forms of electrical conduction covered in earlier lectures, namely by free electrons, and see how metals, semiconductors and insulators differ in this respect. We will then move onto other forms of electrical conduction, such as by diffusion of ions in ionic solids, and by Cooper pairs in superconductors, giving essentially zero resistivity.

1.1   Electrical conductivity by free electrons

Electrons obey the Pauli exclusion principle and cannot occupy the same state. They therefore must occupy a range of energy levels up to a maximum — at 0 K this maximum is well defined and termed the *Fermi energy*, E_F. As the temperature is increased above absolute zero, the distribution of energies smears around the Fermi energy, such that the only vacant energy states can be found around E_F. The behaviour of the electrons around E_F is therefore critical for defining the electrical conductivity (and other properties) of the material.

The outermost electrons in solids can often be modelled as free (or 'nearly free') carriers, in a weak periodic potential from the positive ions in the lattice. The effect of the lattice is to introduce discrete energy bands of allowed electronic states. This further imposes restrictions on the number of free electrons available for electrical conduction.

1.1.1   Metals

In metals, E_F lies within a band of allowed states, so there is no shortage of available carriers for conduction. Conductivity is determined by the scattering properties of the material (mean free path between scattering events) and by the electron velocity between scattering events (the *Fermi velocity*). Electrical conductivity is defined as:

$$ \tag{1.1} $$

where j is the current density (in units of A/m^{-2}) and E is the applied electric field (in units of V/m). The equation of motion for the electron

under an electric field E is:

$$(1.2)$$

We integrate over a period between collisions, τ. On each scattering event, it is impossible to know what the change in electron velocity will be, but we can say that it has some average non-zero value (remember velocity is a vector quantity) otherwise there would be no net current flow. We call this average resultant electron velocity the *drift velocity*, or v_d. This is in contrast to the Fermi velocity, v_F, which is the velocity between scattering events. Thus,

$$(1.3)$$

We can write the time between collisions, τ, in terms of the Fermi velocity and a mean scattering length (or *mean free path*), λ_s.

$$(1.4)$$

Thus:

$$(1.5)$$

$$(1.6)$$

where n is the density of free electrons. Typical values are $\sigma_{Cu} = 10^8$ $(\Omega\text{m})^{-1}$, $v_F = 10^6$ ms^{-1}, $n = 10^{29}$ m^{-3}. These values give a mean free path $\lambda \approx 3.5 \times 10^{-8}$ m, or about 100 atoms. It is therefore not the periodic lattice which is scattering electrons, but deviations from the perfect lattice such as vibrations (which show a linear temperature dependence at elevated temperatures and go away at low temperatures), and impurities/vacancies etc. in the lattice (which show no temperature dependence).
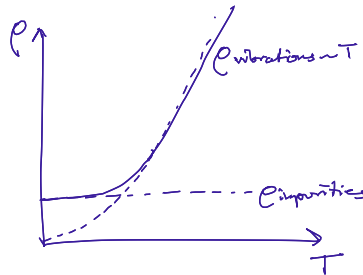

Figure 1.1: The resistivity of a typical metal as a function of temperature
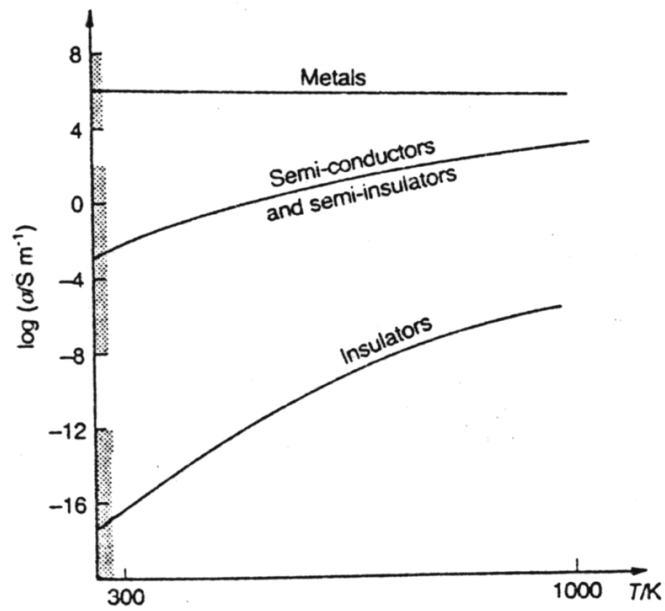
Figure 1.2: Summary of conductivity versus temperature for metals, semi-conductors and insulators. Note the log scale for conductivity.

1.1.2 Semiconductors and insulators

In semiconductors and insulators, the Fermi energy lies in the middle of a band gap — a region of forbidden energy states. At low temperatures there is therefore a negligible number of electrons with sufficient energy to cross the band gap and occupy the higher lying states. The electrical conductivity is therefore determined primarily by the free carrier concentration which depends exponentially on temperature and the band gap energy E_g.

$$(1.7)$$

The distinction between semiconductors and insulators essentially lies in the magnitude of the band gap, compared with room temperature (below about 3.5 eV, materials are generally termed semiconductors). Note that diamond, for example, has a band-gap of 5.5 eV and is an excellent insulator at room temperature. However, at high temperatures it would make a pretty good semiconductor. Semiconductors would be far less interesting if the story ended here. They can be doped with impurities which artificially add free electrons to the material, dramatically altering the conductivity (they can also remove electrons from a full band creating 'holes' with an effective positive charge which are also capable of electrical conduction). It is this property of being able to engineer regions of semiconductor with different conducting properties which has made the semiconductor-based electronics industry possible.
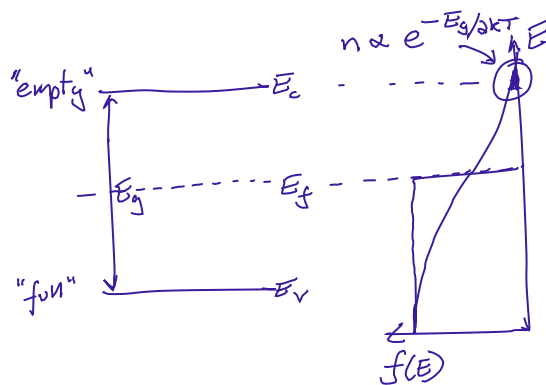

Figure 1.3: The number of free carriers in semiconductors and insulators is exponentially dependent on temperature and the band gap energy

1.2   Electrical properties of alkali halides

In the above section we revised the basic properties of conduction by free electrons, and found that in the case of insulators, the free electron concentration was negligible at room temperature. In this case, other mechanisms may take over, such as conduction by ion transport. In this section we will deal with the electrical and diffusional properties of ionic crystals by looking at a particular example, the alkali halides. The structures of the alkali halides are well known, the most common being NaCl, being describable as two interpenetrating face-centred cubic arrangements of positive and negative ions, the origins of the two substructures being separated by half the cuvic cell edge. We are not concerned with the structure in any detail, except to note that there are equal numbers of positive and negative ions and that the coordination number, Z, is 6 (i.e. each ion has 6 nearest neighbours of the opposite sign).

1.2.1   Intrinsic vacancy density

Clearly, the ability of ions to diffuse through a solid will depend strongly on the concentration of vacancies for it to hop through. We therefore begin by using a thermodynamic argument to estimate the vacancy density.

Recap	Free energy = Internal energy - Temperature $\times$ Entropy

The free energy of the perfect crystal is:

$$\tag{1.8}$$

While the free energy of the actual crystal has additional contributions from the vacancies (let there be N ions and n vacancies *of each sign*, so $2N$ ions and $2n$ vacancies in total):

$$\tag{1.9}$$

Here, ϕ is the total energy of formation for a vacancy *pair*, one on each sublattice, not necessarily adjacent but not too far apart for electrostatic reasons. There are two ways in which the entropy has changed with the introduction of vacancies. The first is the configurational entropy term $S = k_B \ln W$, the second is associated with a change in the oscillator frequency of the ion when it has a vacancy as its nearest neighbour (we define ΔS_{freq} as the change in entropy due to change in oscillator frequency, per ion pair). We have also neglected any volume change created by introducing vacancies, which would produce an additional term pV to the free energy).

5

We differentiate and set to zero to find the equilibrium number of vacancies, making use of Stirling's approximation ($\ln x! \approx x \ln x - x$):

$$(1.10)$$

Making the assumption that $N >> n$, this simplifies to:

$$(1.11)$$

Calculating ΔS_{freq} depends in detail on the model chosen to represent vibrations in the solid, but all models produce the same overall behaviour which is typified by the Einstein model of $3N$ harmonic oscillators per ion for each direction x, y, z.

The entropy of one oscillator with angular frequency ω is given by (see webnotes for a derivation, or a statistical mechanics text book):

$$(1.12)$$

We have $2N$ ions, and thus $6N$ oscillators, so in the perfect crystal:

$$(1.13)$$

In the actual crystal with $2n$ vacancies and coordination number Z, there will be $2nZ$ ions abutting onto vacancies, and so $6nZ$ of these oscillators will have some lower frequency ω':

$$S_a = (6N - 6nZ)\left(k_B + k_B \ln \frac{k_B T}{\hbar \omega}\right) + 6nZ\left(k_B + k_B \ln \frac{k_B T}{\hbar \omega'}\right) \quad (1.14)$$

$$(1.15)$$

Plugging this back into Eq. 1.11, we get:

$$(1.16)$$

Adding a vacancy adjacent to an ion reduces the interatomic forces it experiences, and hence the vibrational frequency drops. Hence $\omega' < \omega$ and we expect C to be greater than 1. The prefactor C is not strongly temperature dependent. Similar expressions for Δ_{freq} can be obtained from other models, but all produce something of the same form as the above. Note also the similarity between the form of this expression, and that of the number of free carriers in intrinsic semiconductors (see Eq. 1.7).

Simple vacancies of the kind described above are not completely free: positive and negative ion vacancies will be attracted to each other as this reduces their electrostatic energy. They may therefore form an associated pair, or even larger aggregates. Such restrictions limit their ability to conduct.

Other defects may be more mobile. For example, consider an associate pair of a (negatively charged) positive ion vacancy and positive ion interstitial (or the inverse version) which is known as a Frenkel defect. As electrical neutrality is maintained locally, there can be unequal numbers of Frenkel pairs of opposite sign. Again the same form of vacancy density results, with an additional correction (N is replaced with $\sqrt{NN_i}$):

$$(1.17)$$

N_i is the number of possible interstitial sites in the crystal (e.g. $N_i = 2N$ for the [4] coordinated sites in fcc).

As with semiconductors, it is possible to *dope* the crystal with defects to artificially increase the number of defects and thus tailor the conducting properties of the material. For example, if a small quantity of $CaCl_2$ is dissolved in NaCl, the resulting crystal has the NaCl structure with the Cl^- sublattice perfect and the Na^+ sublattice occupied at random by (i) a majority of Na^+ ions, (ii) a minority of Ca^{2+} ions and (iii) an equal minority of vacancies. This results in a temperature independent contribution to the number of positive ion vacancies, necessary to preserve the structure, with local electrical neutrality preserved by the Ca^{2+} ions and positive ion vacancies tending to occur close to each other.

1.2.2   Self-diffusion of ions

The ability of particles to diffuse in a medium is characterised by the Diffusion coefficent $\mathcal{D}$, defined as the flux of particles (amount of substance diffusing through some area per unit time) given some concentration gradient (dN/dx).

$$J = -\mathcal{D}\frac{dN}{dx} \qquad (1.18)$$

Einstein showed in 1905 while describing Brownian motion that this was related to the *mobility* of particles, μ, where mobility is defined as the ratio of the drift velocity to the applied force:

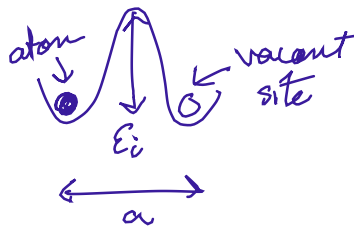| **Einstein relation**	$\mathcal{D} = \mu k_B T$

Figure 1.4: Energy barrier for hopping ion

For electrical conductors where the carriers have charge q, the applied force is qE. Thus,

$$\mathcal{D} = \frac{v_d k_B T}{qE} \tag{1.19}$$

Remembering that $j = n_c q v_d = \sigma E$ (where n_c is the *concentration* of charge carriers), we obtain a relation between the electrical conductivity and the diffusion coefficient:

$$\tag{1.20}$$

We model diffusion of ions in solids as oscillators with frequency ν which are held in their equilibrium position by an energy barrier of height ϵ_i (see Figure 1.4). The probability of jumping to an adjacent site is therefore:

$$\tag{1.21}$$

The probability of that site actually consisting of a vacancy is n/N, and so the above probability must be multiplied by this factor. Following the ordinary laws of kinetic theory, the diffusion coefficient may be shown to be:

$$\tag{1.22}$$

where a is the jump distance. In Eq. 1.16 we obtained an expression for n/N for an intrinsic (un-doped) crystal. We can add to that a term arising from extrinsic doping of defects n_{ext} into the crystal using methods outlined above. Thus:

$$\mathcal{D} = \frac{1}{3} a^2 \nu \exp\left(\frac{-\epsilon_i}{k_B T}\right) \left[\frac{n_{ext}}{N} + C \exp\left(\frac{-\phi}{2 k_B T}\right)\right] \tag{1.23}$$

$$\ln \mathcal{D} = \ln \frac{\nu a^2}{3} - \frac{\epsilon_i}{k_B T} + \ln\left[\frac{n_{ext}}{N} + C \exp\left(\frac{-\phi}{2 k_B T}\right)\right] \tag{1.24}$$
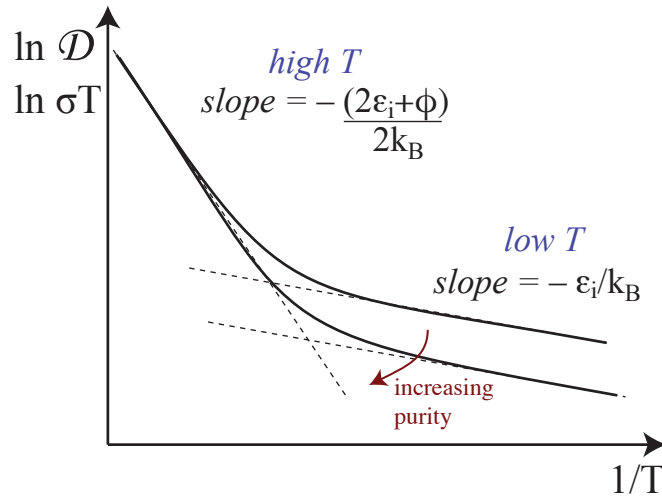
Figure 1.5: The logarithm of D and σT versus reciprocal temperature. Such a plot is termed an Arrhenius plot.

At high temperatures the intrinsic carriers in semiconductors outnumber those from the dopants. Similarly, at high temperatures we can make the approximation that intrinsic vacancies are dominant. Thus, at high temperatures:

$$ \tag{1.25} $$

Conversely, at low temperatures the number of vacancies will be dominated by the extrinsic contribution, and we have:

$$ \tag{1.26} $$

In the two above results, the final term in brackets in a constant with temperature. The dependence of $\ln \mathcal{D}$, and thus $\ln(\sigma T)$, with temperature is therefore $1/T$, with two different slopes in the high- and low-temperature regions. The behaviour is sketched in Figure 1.5. Performing experiments to measure this temperature dependence across a sufficiently wide range therefore allows the determination of ϕ and ϵ_i. For example, values obtained using NaCl for the Na$^+$ ion are:

$\epsilon_i \sim 0.77$ eV $= 1.23 \times 10^{-19}$ J $= 74$ kJmol^{-1}

$\phi \sim 2.06$ eV $= 3.30 \times 10^{-19}$ J $= 198$ kJmol^{-1}
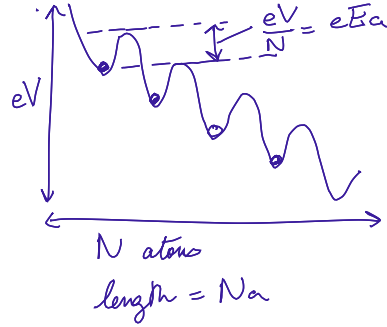
9

Figure 1.6: Energy barrier for hopping ion under the application of a voltage V

1.2.3 Ionic conductivity

The application of an electric field E creates an asymmetry in the potential barrier on either side of the ion by $\pm\frac{1}{2}aEe$, as illustrated in Figure 1.6, so the probability of jumps with, or against, the field become different:

$$ \tag{1.27} $$

$$ \tag{1.28} $$

The rate of charge hopping in any one direction will be $(n/N)p_\pm$, so the resulting current along one conducting chain of ions is:

$$ \tag{1.29} $$

Figure 1.7 shows that for this particular NaCl crystal structure, one chain of ions has effective cross-sectional area of $a^2/2$, so the overall current density is:

$$ \tag{1.30} $$

$$ j = \frac{2}{a^2}e\frac{n}{N}\frac{\nu}{3}\exp\left(\frac{-\epsilon_i}{k_BT}\right)\left[\exp\left(\frac{eaE}{2k_BT}\right) - \exp\left(\frac{-eaE}{2k_BT}\right)\right] \tag{1.31} $$

At realistic electric fields, $aEe << 2k_BT$, and thus we can approximate $\exp(x) = 1 + x....$, giving:
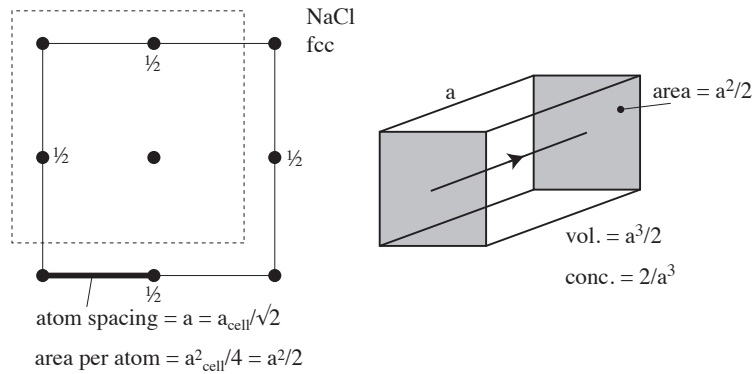
$$ \tag{1.32} $$

10

Figure 1.7: Calculation of area and volume factors for the NaCl fcc structure

Recalling the relationship between σ and $\mathcal{D}$ following the Einstein relation (Eq. 1.20), we can express the above in terms of $\mathcal{D}$ (from Figure 1.7 we see that n_c, the concentration of carriers is equal to $2/a^3$):

$$(1.33)$$

This is identical to the expression used in Eq. 1.22. We have assumed the same species / same mechanism is responsible for diffusion and conduction. Deviations from the Einstein relation indicate the breakdown of this assumption.

1.2.4   Which ion conducts?

The theory above was derived for the case of vacancies of one type of site being responsible for all conduction. Generalisation to mixed conductivity is only an algebraic difficulty. However, it is possible to experimentally determine the relative importance of the two processes of conduction by positive or negative ions. Two weighed slabs of salt M^+X^- are pressed together between two weighed electrodes of the metal M. Electric current is passed through the cell. In the two extreme cases (see Figure 1.8):

a. If only positive ions conduct (i.e. via positive ion vacancies) the cathode [4] will grow at the expense of the anode [3]. The slabs of salt will remain unchanged in size, acting purely as conduction paths.

b. If only negative ions conduct (again via a vacancy mechanism) the X^- ions are neutralised at the anode [3] and form new layers of salt M^+X^- by dissolving the metal. The salt layers are added to block [1] while
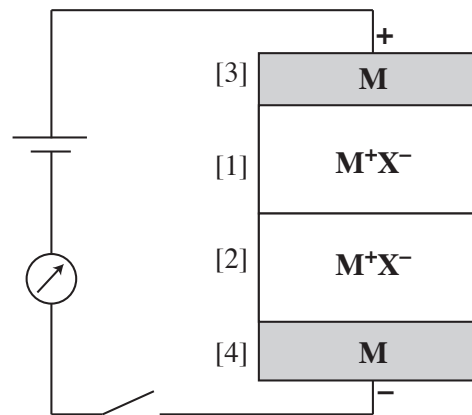
Figure 1.8: Schematic of experiment used to determine relative contributions of positive and negative ions to electrical conductivity

+ve ion dominates	-ve ion dominates
akali halides: Li, Na, K, Rb, Cs F, Cl, Br, I	other halides: Pb, Ba
silver halides	

Table 1.1: Dominant ions for electrical conductivity in various ionic solids

the anode [3] decreases in weight. At the cathode [4], an equivalent number of metal ions M^+ are deposited as neutral atoms from the salt layers close by. Thus, salt block [2] also decreases in weight (efflux of X^- and deposition of M^+ and the cathode [4] grows.

Weighing the electrodes and salt blocks before and after a measured quantity of electric charge has passed through the cell (checking for consistency via Faraday's Law and relative atomic masses) enables the proportions of conductivity modes to be deduced in the mixed case. In the alkali halides, the ion current is carried mainly by the positive ions, as is the case with the silver halides.
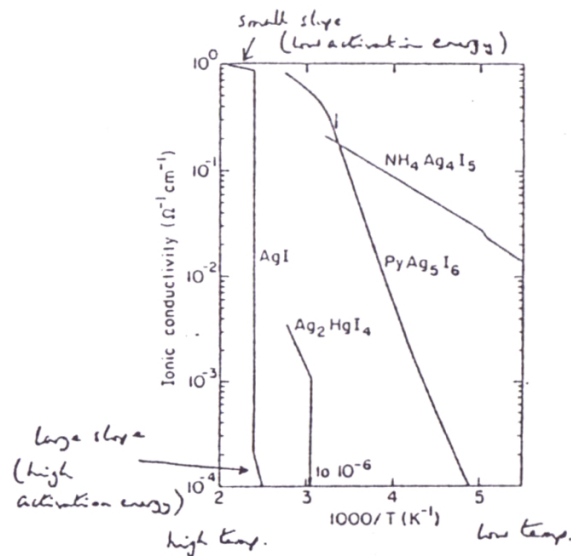
Figure 1.9: Ionic conductivity versus temperature in various superionic materials

1.3 Superionic conductors

A subset of ionic conductors which have attracted particular interest are the *superionic conductors* (or *fast-ion* conductors). As the name implies, they have a very large conductivity compared with normal ionic conductors. The temperature dependence of some examples is shown in Figure 1.9. One of the most spectacular examples is silver iodide AgI: at the superionic transition its conductivity increases by more than $\times 5000$. There is a corresponding decrease in the apparent activation energy for hopping ϵ_i — this is a key characteristic of the class of superionic conductors.

The transition is associated with a crystallographic phase change. The "super"-phase must have a transport mechanism which is especially efficient (e.g. via interstitial sites such as those illustrated in Figure 1.10). In the α-AgI structure there are 24 tetrahedral interstitial sites through which the smaller positive Ag^+ ion may move rapidly through the bcc lattice of I^- ions. The structure is thus somewhat analogous to liquid crystals (covered later in this course) — the lattice has partially melted (we can call it pseudo-molten with respect to Ag^+, crystalline with respect to I^-).

13

- ● 'Tetrahedral' site
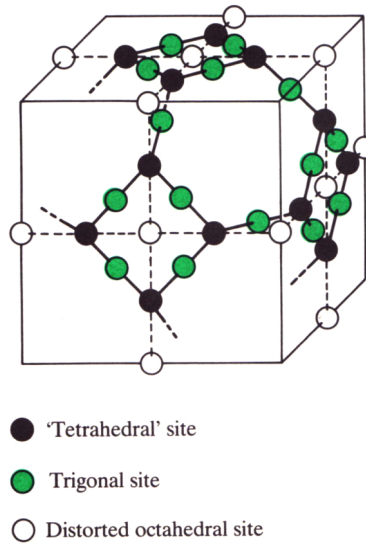- ● Trigonal site
- ○ Distorted octahedral site
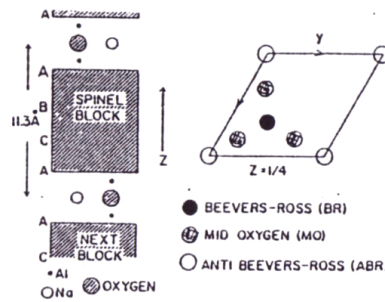
Figure 1.10: α-AgI structure

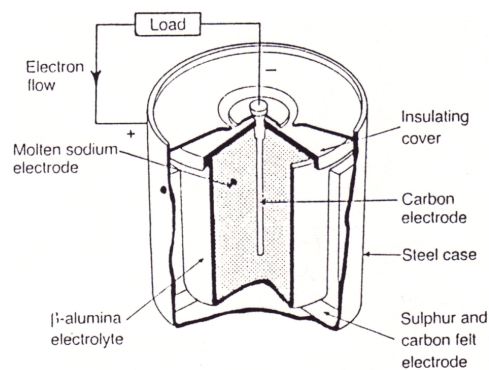Figure 1.11: Sodium β-alumina electrolyte

Figure 1.12: Schematic of an Na-S cell (courtesy of Chloride Silent Power)

14

1.3.1   Sodium-sulphur battery: Na β-Al$_2$O$_3$ electrolyte

Technologically one of the most important superionic systems may be sodium β-alumina (e.g. Na$_2$O.11Al$_2$O$_3$) for use in the sodium-sulphur high temperature battery. Spinel blocks of Al^{3+} and O^{2-} are separated by Al-O-Na conducting planes as shown in Figure 1.11. The Na$^+$ ions in the conducting planes are disordered and can move rapidly from site to site, giving the high conductivity. In the context of the Na-S battery, the fact that the Na is transported (as well as the electric charge) is not a problem — in fact, it is what's needed for a battery to function.

A schematic of a Na-S battery is shown in Figure 1.12. Molten sodium in the centre of the cell releases sodium ions into the electrolyte and electrons to the electrode. The sodium ions react with sulphur at the other electrode taking up electrons. An EMF ξ is produced, defined as the energy gained per unit charge:

$$(1.34)$$

ΔG is the standard free energy (in units of J mol-1), z is the charge of the ion (e.g. $+1$, $+2$ etc.), and F is the Faraday constant (defined as the electron charge e times Avagadro's number N_A such that $F = 96400$ Cmol^{-1}).

$$(1.35)$$

a_i is the activity (a measure of effective concentration) of a species at the electrodes on either side of the electrolyte. Thus,

$$(1.36)$$

For an Na-S cell, the EMF is 2.7 V.

1.4   Electron hopping (polaron) conduction

An alternative *electron* conduction mechanism may also play a role in certain impure (or deliberately doped/alloyed) ionic solids if the metal cation can exist in different ionisation states (e.g. if it is a transition metal). As an illustration, if Li$_2$O is added to NiO and the mixture fired under oxidising conditions then the resulting crystal structure is found to contain Li$^+$, Ni^{2+} and Ni^{3+} on the "Ni" sites of the NiO structure as indicated in Figure 1.13. An electron hopping from a Ni^{2+} ion to an adjacent Ni^{3+} ion transfers negative charge in the direction of the hop and swaps the occupancy of the site
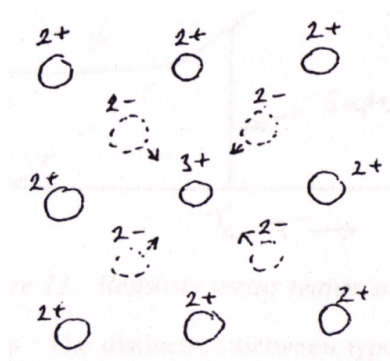
Figure 1.13: A *polaron* consists of an excess bound charge and associated polarisation of nearby ions

Poly(p-phenylene vinylene) 'PPV'	2.4 eV	$\sim$520 nm
Polyacetylene	1.5-1.7 eV	$\sim$780 nm
Polyisothianaphtene	1.0-1.2 eV	$\sim$1120 nm

Table 1.2: Some example band gaps for conducting polymers

in a way analogous to that of an ion hopping into a vacancy. Likewise, there will be an activation energy associated with the transfer and so on. Again, there will be a logarithmic dependence of the diffusion coefficient with $1/T$, as shown in Figure 1.5.

The term *polaron* is sometimes used because the Ni^{3+} ion, being positive with respect to the expected Ni^{2+} ion, polarises the surrounding oxygen ions. It is this composite entity which should be considered, not just electron transfer between bare ions.

1.5 Conducting polymers

Typical organic polymers where the carbon atoms exhibit sp^3 hybridization are good insulators (e.g. PVC). However, in certain classes of polymer where there are alternating single-double bonds along a carbon backbone exhibit sp^2 + p_z hybridization and there is the possibility of *delocalised* π-bond formation along the chain involving the p_z orbitals. The simplest example of such a *conjugated* polymer is polyacetylene (see Figure 1.14). Their behaviour is much like semiconductors, where excitation across a band gap is required to promote electrons to a delocalised energy where they are capable of electrical conduction. Some typical band gaps are given in Table 1.2 below.

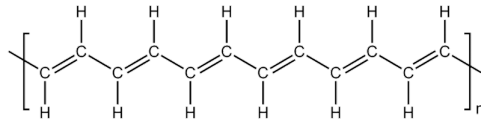Conducting polymers can be doped, just like traditional semiconductors.

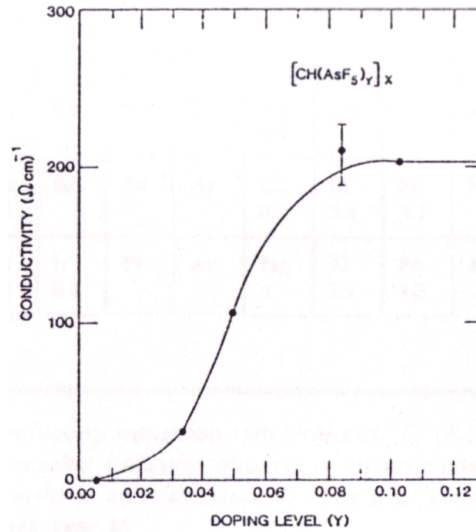Figure 1.14: Structure of the most basic conjugated polymer: polyacetylene

Figure 1.15: Conductivity of polyacetylene doped with AsF_5

17

This can be performed by adding electron-withdrawing or -donating side-chains to the polymer, or through electrochemical doping, or through a redox agent. Figure 1.15 shows how the conductivity of polyacetylene varies with AsF_5 doping concentration.

Polymer-based LED technology is an exciting way in which these materials are being exploited to yield flexible displays with vibrant colours. PPV or poly (*p*-phenylenevinylene) is widely used in this context. Electrons are injected from a negatively biased metal electrode (e.g. Ca or Al) and holes injected from a semi-transparent electrode (e.g. indium tin oxide, ITO). The electrons and holes recombine within the polymer *radiatively*, emitting a photon at a wavelength given by the bandgap of the polymer. There are several processing advantages to polymer LEDs, and cost is widely touted as an advantage though it is difficult to challenge the remarkably efficient semiconductor industry in this regard. One major challenge which polymer LEDs have faced is the often short lifetimes of the devices, though there has been much progress in this area in recent years and several polymer based products (including large flat screen TVs) are now on the market.

1.6   Superconductivity

The successful liquification of helium at the beginning of the 20th century opened the doors to a new temperature regime in which to explore the properties of materials. There was considerable disagreement, for example, regarding what would happen to the resistance of metals as the temperature approached absolute 0. Metals such as Cu, which are good conductors at room temperature, where first measured. These showed a behaviour consistent with Figure 1.1 — scattering by impurities and defects dominated the low temperature resistance of the material. Then in 1911, Kamerlingh Onnes began studying mercury as it could be more readily purified. His remarkable discovery was that rather than a gradual change with temperature, there was a sudden transition in the material to a state which appeared to have *zero resistance*.
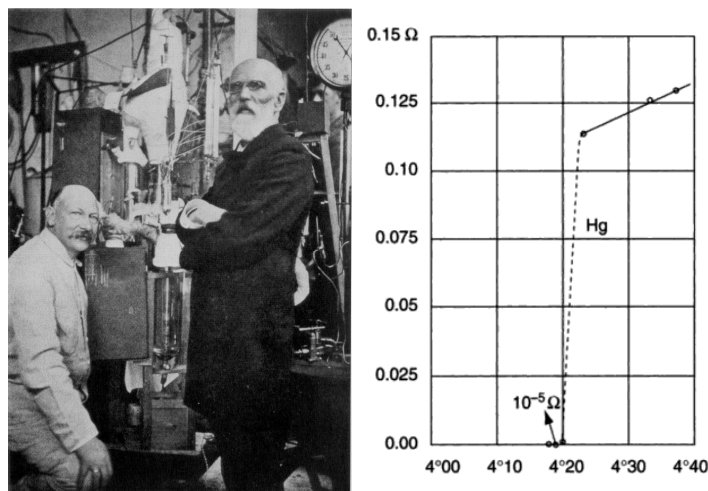

Figure 1.16: Heike Kamerlingh Onnes (left) in Leiden was the first to liquify helium in 1908, which then led to the discovery of superconductivity three years later. Also in the photo is Johannes Diderik van der Waals (right). On the right is the plot of the measured resistance of a mercurcy sample as a function of temperature, as measured by Kamerlingh Onnes

1.6.1   What is the resistivity of a superconductor?

Experiments have been conducted since the 1950s which measure the decay time for a current which has been established in a superconducting ring. For example, in 1961 a decay time of $> 10^5$ years was established (within

experimental error), providing an upper limit of 4×10^{-25} Ωm for the supeconducting resistivity. Subsequent experiments have measured limits down to $\sim 10^{-29}$ Ωm. These numbers can be contrasted with a good conductor such as copper, which does not superconduct: $\rho(4.2 \text{ K}) = \sim 7 \times 10^{-13}$ Ωm.

1.6.2 Superconducting elements

The table below shows the distribution of superconductivity amongst some of the elements. In addition, there are many hundreds of alloy systems which are superconducting, and indeed it is these that are generally of most interest for practical applications.

Table 1.3: Some of the superconducting elements and their superconducting transition temperature, T_c in Kelvin in zero applied magnetic field for "pure" material. Boxes edged in single lines are Type I, double lines are Type II.

1.6.3 Magnetic field effects on superconductors

The excitement experienced by early researchers having discovered resistanceless conductivity is palpable. However, it soon became clear that some of the applications one would envisage for this type of material were limited — passing a modest current or applying a modest magnetic field was enough to turn the material back into the *normal state*. Therefore, in addition to a critical transition temperature T_c, superconductors can be characterised by critical magnetic field and critical current values.

Twenty years later, Meissner discovered another fundamental property of superconductors which differentiated them from a simple 'perfect' conductor. Material in a superconducting state completely expels an applied magnetic field — in other words it behaves as a perfect diamagnet. This is known as

the *Meissner effect*, and illustrated in Figure 1.17. A perfect conductor will have no internal electric field — Ohm's law tells us $E = \rho j$, so $\rho \to 0$ implies $E \to 0$. One of Maxwell's equations (discussed in detail later in this course) relates the time variation of the magnetic field to the spatial variation of the electric field:

$$\textbf{Maxwell 3} \qquad \frac{\partial E_x}{\partial z} = -\frac{\partial B_y}{\partial t}$$

Given $E = 0$, this tells us that a perfect conductor must have $\partial B/\partial t = 0$, but not necessarily $B = 0$. Hence, when a material which becomes perfectly conducting below T_c is placed in a magnetic field and cooled through T_c , the B field in the material stays constant, and is not expelled. On the other
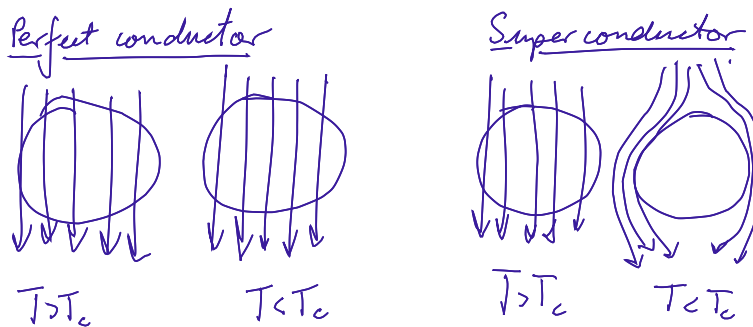

Figure 1.17: Magnetic field lines around a perfect conductor, and a superconductor, above and below the critical temperature

hand, when a superconductor is placed in a field and cooled through T_c, the magnetic field is expelled upon transition to the superconducting state. In other words the material acquires a magnetisation, carried by surface current loops, which is equal and opposite to the applied field. Such currents must be maintained *ad infinitum*, so for a material to be a perfect diamagnet in this way it must also have zero resistance.

1.6.4   Magnetisation curve

For a specimen in the shape of a long thin rod with a magnetic field applied parallel to its length, the geometry is termed "ideal". The magnetisation curve for such a specimen is shown in Figure 1.18, where H is plotted against $-M$ (the magnetisation *opposes* the applied field). We'll concentrate first on what are termed *Type I* superconductors shown on the left of the figure. Following the Meissner effect, the magnetisation of the sample exactly opposes the applied field, so $-M = H$ up until a critical field, H_c. Above this field,

superconductivity is destroyed and the material returns to the normal state. Correspondingly, the resistivity (also plotted in Figure 1.18) becomes finite at fields about H_c. In the ideal case, the magnetisation path is completely reversible. The work done by the superconductor in expelling the applied
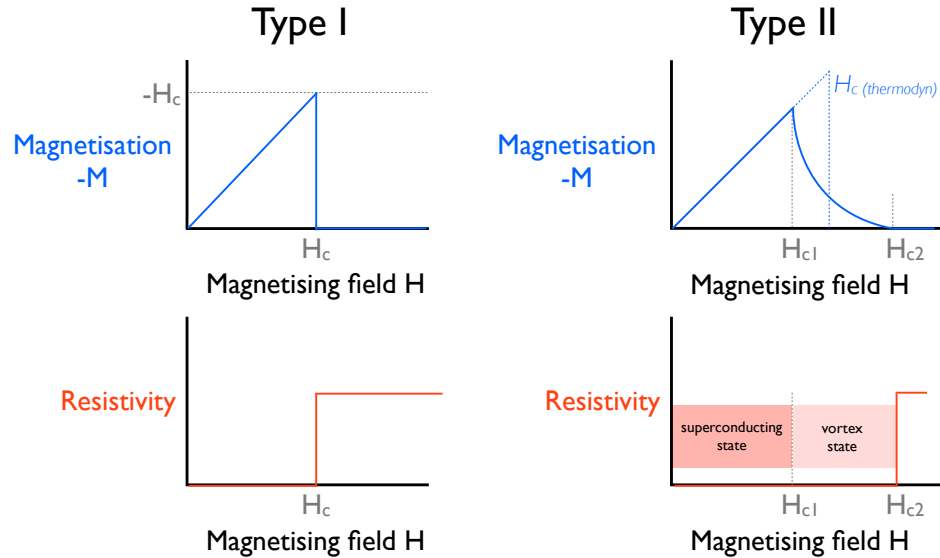

Figure 1.18: Magnetisation and resistivity curves for Type I and Type II superconductors, as a function of magnetising field H, below T_c

field is the area under the magnetisation curve of M vs B (where $B = \mu H$). Once this energy reaches a certain point, the superconducting state no longer becomes favourable for the material, and it turns normal. If we call the free energy difference between the superconducting state and the normal state ΔG_{super} (per unit volume), we can write:

$$\tag{1.37}$$

Based on this magnetic field dependence, there are clearly implications for the maximum current that can be passed through a superconductor which we will examine in a subsequent section.

1.6.5 Type I vs Type II superconductors

So far we have described the properties of so-called Type I superconductors, which we can think of as ideal, pure superconductors. A technologically more interesting class is the *Type II* superconductors, whose magnetic field

dependence is shown on the right-hand part of Figure 1.18. We see two distinct critical fields H_{c1} and H_{c2}. For fields up to H_{c1}, the Meissner effect still holds and the applied field is completely expelled, just as for a Type I material. However, as the field is raised above H_{c1}, the magnetisation falls off gradually until H_{c2} where it drops to 0. The resistivity remains zero until H_{c2}, above which it becomes finite and the material returns to the normal state. It is still possible to define the *thermodynamic critical field H_c* for Type II materials such that the area under the *M-H* curve is $1/2$ H_c^2, which must lie between H_{c1} and H_{c2}. Type II materials tend to be alloys, or transition metals with high values of resistivity in the normal state (see Figure 1.3). Furthermore, the magnetisation curve depicted for Type II materials is idealised, and one would expect some hysteresis in real materials.

The magnetisation behaviour of Type II superconductors is explained by the penetration of magnetic flux into the material, creating small puddles of normal material within a superconducting bulk. The material is said to be in the *mixed state* or *vortex state*. Because the bulk of the materials remains in the superconducting state, there remain conducting pathways of zero resistance, and hence the resistivity remains zero until the bulk turns normal at H_{c2}. The magnetic flux penetrates the material in discrete quanta Φ_0, with a small screening current induced in the surrounding superconducting material — hence, a *vortex*.

1.6.6 Flux quantisation

The derivation of the quantisation of flux into multiples of Φ_0 lies beyond scope of this course. However, there is a nice argument based on the *Aharonov-Bohm effect* which illustrates the idea, as depicted in Figure 1.19. The
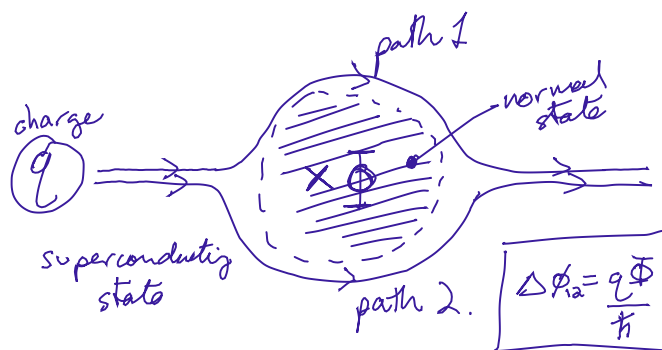

Figure 1.19: An illustration of the Aharonov-Bohm effect: in the absence of scattering, a charge carrier will pick up different phases depending on which path it takes around some flux.

Aharonov-Bohm effect states that if we have two current paths, carried by a charge q, around either side of some flux Φ, and there is *no scattering*, then the phase difference $\Delta\phi$ of the two paths is:

$$\Delta\phi = \frac{q\Phi}{\hbar} \tag{1.38}$$

If the two paths interfere in any way other than perfectly *constructively*, then the presence of the flux appears as a source of scattering, which the superconductor does not permit. We can therefore state that the superconductor will only allow flux penetration in units where the two paths interfere constructively, i.e. their relative phase must be a multiple of 2π.

$$\Delta\phi = \frac{q\Phi}{\hbar} = 2N\pi \qquad \text{and thus,} \qquad \Phi = \frac{Nh}{q} = N\Phi_0 \tag{1.39}$$

So the allowed flux is quantised in units of $\Phi_0 = h/q$. We can measure the flux quantum to be:

$$\Phi_0 = \frac{h}{2e} = 2 \times 10^{-15} \text{ Weber} \tag{1.40}$$

So, the charge carriers in superconductors appear to have a charge of *twice* the electric charge... the entities responsible for electrical conduction in superconductors are electron pairs, known as *Cooper pairs*. If it seems counterintuitive that electrons should pair up in this way, don't be discouraged — it was not until 46 years after the discovery of the phenomenon that a satisfactory theory for superconductivity was put forward! The paired state, where two electrons couple to the same lattice vibration, becomes energetically favourable below T_c. Electrons paired in this way cannot be readily scattered, hence the resistance-less current flow.

1.6.7   The flux lattice

Using very small amounts of powder and replica techniques for the electron microscope, several research groups have imaged the flux lattice emerging from the surface of a Type II superconductor by decorating it with ferromagnetic powder particles. More recently, the use of scanning tunneling microscope (STM) at cryogenic temperatures has enabled the direct imaging of the regions of normal state of the material, and thus the flux lattice (see Figure 1.20. The flux lattice is triangular, and has a lattice constant which decreases as the applied field increases. As with atomic lattices, movements of flux-lattice dislocations, vacancies etc. are important to understand the behaviour of the superconductor, especially when a field gradient is applied.
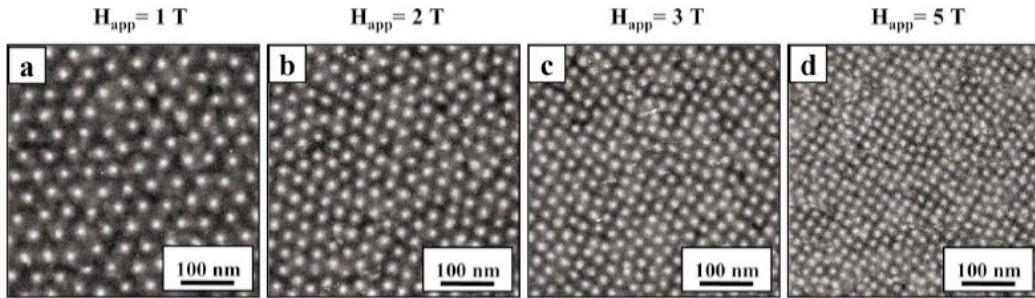
Figure 1.20: Scanning tunneling microscope images of the vortex lattice of a Type II superconductor as a function of applied magnetic field at 2.3 K [Courtesy of the Electron Physics Group at NIST]

In high-temperature ceramic superconductors there is much discussion on whether the flux distribution is amorphous or glassy in nature, and whether it has a 'melting' temperature in the region of 30 K.

1.6.8 Critical current

We have already seen that there is a critical field above which a superconductor is driven into the normal state. It follows that if we try to drive too great a current along a superconductor, the associated magnetic field will exceed H_c and the material goes normal. For Type I materials, the critical current I_c is simply that which generates the critical magnetic field at the surface. For a long thin wire of radius r, it follows directly from Ampère's Law ($H = I/2\pi r$) that:

$$(1.41)$$

However, the low value of H_c in Type I materials restricts their use in applications such as superconducting magnets. In Type II materials, where flux is allowed to penetrate the material, the situation is more interesting. Let us consider current through a Type II superconductor in the mixed state, in the geometry shown in Figure 1.21 where there is a magnetic field running perpendicular to the current. There is a Lorentz force on each electron of $-ev_x \times B_y$. This force therefore acts along z, and has the following magnitude per unit volume of material (where n is the electron concentration and N is the number of flux quanta per unit area):

$$(1.42)$$

The current density $j = -nev_x$, so this can be rewritten as:
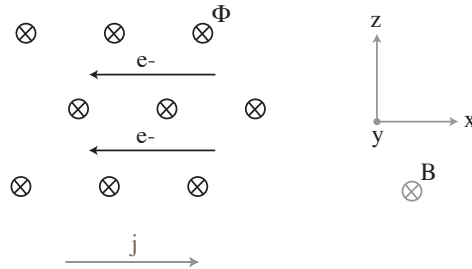
$$(1.43)$$

Figure 1.21: The effect of current on flux quanta

There must be an equal and opposite force on the flux lines. So if we apply a fixed current j along the sample, each flux quantum experiences a force $j\Phi_0$ in a direction perpendicular to the current flow. If these flux lines are allowed to move under this force, we have a time-varying magnetic field, and by the same Maxwell's equation used above, an induced voltage (electric field per unit distance)

Maxwell 3	$\dfrac{\partial E_x}{\partial z} = -\dfrac{\partial B_y}{\partial t}$

Thus, we have an induced voltage which is proportional to the current through the material — it looks like a resistor. Materials in the mixed state with no *flux pinning* are therefore not capable of carrying much current.

1.6.9 Flux pinning

If the force derived above is insufficient to move the flux line through the material, it is possible for a large current to flow without resistance. By equating this pinning force to that derived above, we obtain:

$$(1.44)$$

This argument is oversimplified, neglecting (i) the fact that the flux lines through the material are precisely due to the applied current in the first place and (ii) the effects of interactions between flux lines, amongst other things. However, it does illustrate the critical role which flux pinning plays in enabling superconductors to carry large currents and make them technologically useful. In looking for suitable materials from which to fabricate a high-field magnet, for example, we therefore require something with a combination of:

a. large flux pinning

b. high value of H_{c2}

26

High temperature / high field alloys

Alloys tend to be Type II materials. Examples include:

	T_c (K)	B_{c2} (T)
Nb40-Ti60	9	10
Nb_3Sn	18.5	20
$Nb_3(Ge_{0.8}Al_{0.2})$	10	
Chevrel phases	10	60

Table 1.4: Some superconducting alloys and compounds and their properties

There is still much basic research to be done into the underlying mechanisms of both these properties and so at present these qualities are mainly empirical as we shall see when discussing actual materials in the following section. A Type II superconductor is termed *hard* if the flux lines within it experience a high pinning force.

1.6.10 Superconducting materials

Tables 1.4 and 1.5 survey some example values for critical temperature and field in Type II superconductors. There is a very approximate correlation between T_c and H_c, but as seen from the Chevrel phase materials this doesn't always hold. The whole panoply of complication of the metallurgical phase diagram spills over into superconductivity parameters such as T_c, as different phases become stable in different composition ranges. Most of the work on the alloys described in Table 1.4 was done before the 1980s, when attention shifted towards the higher-T_c ceramic materials. Note that as usual, the application of these materials lags a decade or so behind their discovery.

In the 1980s, superconducting ceramic metals with 'high' critical temperatures was discovered and they continue to attract considerable attention. Their general formula is $(L_xM_{1-x})_mA_nD_p$, where L is usually a rare earth, M an alkali earth, A is Cu (part 2+, part 3+) and D is oxygen. Some examples are shown in Table 1.5.

1.6.11 Organic superconductors

There is also renewed interest in superconductors based on organic materials. Although the values of T_c and J_c are typically very low, they provide a useful test bed to explore theories and subsequently improve the characteristics of

High temperature ceramic superconductors

	T_c (K)	structure	
$(La_{2-x}Ba_x)CuO_{4-y}$	33	K_2NiF_4 structure	(Nobel Prize 1987)
$YBa_2Cu_3O_7$	93	layered perovskite	
$Bi_2Sr_2CaCu_2O_m$	96	layer	
$(Bi_{1-x}Pb_x)_2Sr_2Ca_2Cu_3O_{11}$	110	layer	
$TlBa_mCa_nCu_pO_y$	up to 125	layer	

Table 1.5: Some superconducting ceramic materials and their properties

other superconductors. An example is the layered charge transfer salt shown in Figure 1.22 where the current runs along the layers of $Cu(CSN)_2$.
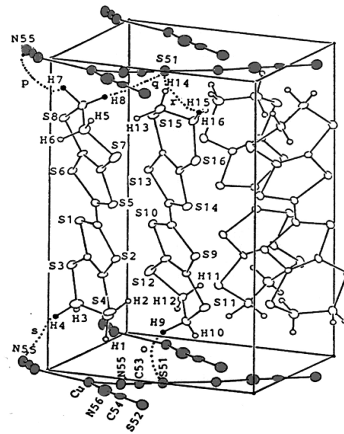

Figure 1.22: An example organic superconductor: k-BEDT-TTF$_2$Cu(CSN)$_2$

1.6.12 Superconducting materials for high field magnets

Following the arguments described earlier, the critical current must depend on temperature and externally applied magnetic field. For a fixed temperature, applying an external magnetic field causes the critical current to fall. However, curves of J_c vs H for traditional 'hard' Type II materials typically exhibit a plateau, and sometimes even a peak effect. Figure 1.23 shows an example for the 75Zr-25Hb alloy. In its purest (recrystallised) state it exhibits no plateau, just a reasonable monotically decreasing value of J_c with increasing H. This is consistent with the flux in the material being due to the combination of a term induced by current through the superconductor, plus

an applied external field. The same material, only partially recrystallised after cold work has a much higher value of J_c at elevated fields. The highest values of all for this system are found after cold work and a particular heat treatment, the latter probably involving some precipitation due to the presence of oxygen. If the scale of the precipitation, or of the dislocation tangles in polygonised walls, is right, then large pinning (and high J_c) results.

The curve of Figure 1.23 is typical of superconducting wires for applications in high-field magnets. Such curves are constantly being revised as manufacturers vie with each other to produce better and better wires. The first generation of wires were NbZr and NbTi (mostly the latter is used now, for example in the LHC in CERN). A second generation is Nb_3Sn, which is used, for example, in fusion energy research.
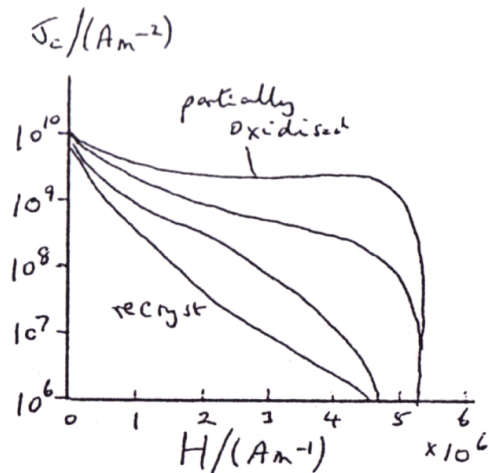

Figure 1.23: Critical current density J_c versus applied field H